

Direct atomic layer deposition of ultrathin aluminium oxide on monolayer MoS₂ exfoliated on gold: the role of the substrate

Emanuela Schilirò, Raffaella Lo Nigro, Salvatore E. Panasci, Simonpietro Agnello, Marco Cannas, Franco M. Gelardi, Fabrizio Roccaforte, Filippo Giannazzo**

Dr. E. Schilirò, Dr. R. Lo Nigro, S. E. Panasci, Prof. S. Agnello, Dr. F. Roccaforte, Dr. F. Giannazzo
CNR-IMM,
Strada VIII, 5 95121, Catania, Italy
e-mail: filippo.giannazzo@imm.cnr.it
raffaella.lonigro@imm.cnr.it

Prof. S. Agnello, Prof. M. Cannas, Prof. F. M. Gelardi
University of Palermo, Department of Physics and Chemistry Emilio Segrè,
Via Archirafi 36, 90123 Palermo, Italy

Prof. S. Agnello
ATeN Center, University of Palermo,
Viale delle Scienze Ed. 18, 90128 Palermo, Italy

S. E. Panasci
Department of Physics and Astronomy, University of Catania,
Via Santa Sofia 64, 95123 Catania, Italy

Keywords: MoS₂, atomic layer deposition, AFM, C-AFM, Raman, Photoluminescence

Abstract

In this paper we demonstrated the thermal Atomic Layer Deposition (ALD) growth at 250 °C of highly homogeneous and ultra-thin (~3.6 nm) Al₂O₃ films with excellent insulating properties directly onto a monolayer (1L) MoS₂ membrane exfoliated on gold. Differently than in the case of 1L MoS₂ supported by a common insulating substrate (Al₂O₃/Si), a better nucleation process of the high-*k* film was observed on the 1L MoS₂/Au system since the ALD early stages. Atomic force microscopy analyses showed a ~50% Al₂O₃ surface coverage just after 10 ALD cycles, its increasing up to >90% (after 40 cycles), and an uniform ~3.6 nm film, after 80 cycles. The coverage percentage was found to be significantly reduced in the case of 2L MoS₂/Au, indicating a crucial role of the interfacial interaction between the aluminum precursor and MoS₂/Au surface. Finally, Raman spectroscopy and

PL analyses provided an insight about the role played by the tensile strain and p-type doping of 1L MoS₂ induced by the gold substrate on the enhanced high-*k* nucleation of Al₂O₃ thin films. The presently shown high quality ALD growth of high-*k* Al₂O₃ dielectrics on large area 1L MoS₂ induced by the Au underlayer can be considered of wide interest for potential device applications based on this material system.

Introduction

Semiconducting transition metal dichalcogenides (TMDs), including MoS₂, WS₂, MoSe₂ and WSe₂, are currently widely investigated for next generation electronic and optoelectronic applications [1,2]. The deposition of high-*k* dielectrics thin films (such as Al₂O₃ and HfO₂) on the TMDs surface represents a key requirement for the fabrication of electronic devices [3,4,5]. As an example, the deposition of a HfO₂ gate insulator (~30 nm thick) on top of monolayer (1L) MoS₂ represented the enabling step to demonstrate a field effect transistor (FET) with excellent on/off ratio (~ 10⁸), nearly ideal sub-threshold swing (~ 70 mV/dec) and high room temperature electron mobility (>200 cm²V⁻¹s⁻¹), due to the efficient reduction of charged impurities scattering because of the high-*k* dielectric film [6]. Similarly, an Al₂O₃ top gate dielectric (~16 nm thick) was employed for the demonstration of a high mobility (~125 cm²V⁻¹s⁻¹) multilayer MoS₂ transistor [7]. In all these cases, the high-*k* dielectric films were grown by the atomic layer deposition (ALD) technique [8], commonly employed in microelectronics to obtain uniform and conformal insulating films with a sub-nanometric control of the thickness. Ideally, layer-by-layer deposition of ultra-thin films requires the presence of a sufficiently high and uniform density of dangling bonds, necessary for precursor chemisorption on the sample surface in the early stages of the ALD process [9,10]. However, the inherent lack of out-of-plane bonds in two-dimensional (2D) layered materials represents an obstacle for an ideal ALD growth, resulting in an inhomogeneous coverage especially for very thin (<10 nm) deposited films [11,12]. In this context, relatively thick high-*k* films were employed in the first pioneering studies on

MoS₂ transistors to achieve a uniform coverage of MoS₂ surface, thus minimizing the gate leakage current. However, the real application of MoS₂ FETs in next generation logic devices requires an aggressive scaling of the channel length and, consequently, of the high-k dielectric thickness [3]. Hence, several strategies have been investigated in the last few years to improve the ALD growth on TMDs, by tailoring the process conditions and/or by appropriate pre-functionalization treatments of the surface. Many of these approaches were inspired by ALD growth experiments performed on graphene [13,14,15]. As an example, *Park et al.* [10] systematically investigated thermal ALD of Al₂O₃, using trimethyl-aluminum (TMA) as the Al precursor and water (H₂O) as co-reactant, on the surface of different TMDs, i.e. MoS₂, WS₂ and WSe₂ multilayers. The deposition temperature (T_{dep}) and the TMA adsorption energy (E_{ads}) on the TMDs surface were demonstrated to play a crucial role on the uniformity of the deposited Al₂O₃ (~10 nm) films. In particular, E_{ads} , which is related to the substrate polarizability, was found to be larger for W- and Se-based TMDs (e.g., WS₂ and WSe₂) than for MoS₂. Furthermore, while inhomogeneous Al₂O₃ films (with a large density of pinholes) were obtained at typical deposition temperatures from 200 °C to 250 °C, the coverage uniformity was highly improved by lowering T_{dep} to 150°C, i.e. reducing the desorption of the metal precursors from the MoS₂ surface [10]. Similarly to the strategy used on graphene [16], a two-steps ALD process, consisting in the low temperature (80 °C) deposition of an ultrathin AlO_x layer, followed by a second ALD step at higher temperature (180 °C), was employed to obtain a homogeneous Al₂O₃ film with <10 nm total thickness on MoS₂ [17]. Despite the use of a reduced temperature at the beginning or during the whole ALD process can be beneficial to improve the coverage uniformity, it may result in a lower dielectric quality due to a reduced reactivity of the ALD-precursors [18]. Another strategy to improve the ALD growth on MoS₂ surface has been to replace H₂O with a more reactive co-reactant, such as ozone (O₃), which allowed to obtain uniform Al₂O₃ layers (~5 nm thick) at a temperature of 200 °C [19]. Alternatively, an O₂-plasma pre-treatment of multilayer MoS₂ surface, resulting in the formation of an ultrathin Mo-oxide layer, was shown to significantly improve the uniformity of the deposited Al₂O₃ or HfO₂ films as compared to the case of pristine MoS₂ [20]. More recently, water

plasma pre-treatments of the MoS₂ surface have been used to create hydroxyl groups for conventional thermal ALD at 200 – 250 °C, resulting in the deposition of uniform Al₂O₃ films with thickness down to 1.5 nm [21]. In spite of these beneficial effects, the damage and chemical modifications introduced by these plasma pre-treatments can affect the electronic transport in MoS₂ devices. Besides thermal ALD, plasma-enhanced ALD (PEALD) processes have been also recently investigated to grow very thin films (<5 nm) of Al₂O₃ and HfO₂ on MoS₂ samples with different layer numbers [22,23]. In particular, electrical characterization of 1L, 2L, and 3L MoS₂ back-gated transistors before and after HfO₂ PEALD revealed the occurrence of plasma damage, resulting in significant degradation of the electronic properties especially for 1L MoS₂ [23].

In addition to these processes involving a chemical modification of MoS₂ surface, non-covalent functionalization with thin organic (e.g., perylene derivatives) [24] or inorganic (e.g., SiO₂ nanoparticles) [25] seeding layers has been also explored to promote the thermal ALD growth of thin Al₂O₃ films on MoS₂. However, the use of these interlayers ultimately limits the minimum thickness of the dielectric and may affect the electrical quality of the interface.

This short overview about ALD of high-*k* dielectrics on TMDs indicates that the seeding layers and pre-functionalization approaches explored so far presents some disadvantages, while direct thermal ALD of ultra-thin films would be highly desirable. In this respect, the interaction of atomically thin MoS₂ layers with the underlying substrate is expected to play an important role in the ALD nucleation stage, similarly to what observed for monolayer graphene residing on some specific substrates [26,27]. As an example, *Dlubak et al.* [26] reported an enhanced Al₂O₃ nucleation on CVD-grown 1L graphene residing on the native metal substrates (Cu, Ni), that was ascribed to an improved ALD-precursor adsorption due the electrostatic effect of polar traps located at graphene/metal interface [28,29]. More recently, the uniform growth of ultra-thin (~2.4 nm) Al₂O₃ films by direct thermal ALD (at 250 °C) on monolayer epitaxial graphene on 4H-SiC(0001) has been ascribed to the beneficial effect of the carbon buffer layer at the interface with the substrate [30]. To the best of our knowledge, analogous substrate effects on the ALD nucleation onto 1L TMDs have not been reported so far.

In this paper, we investigated the ALD growth of ultra-thin (<4 nm) Al_2O_3 films on 1L MoS_2 produced by gold assisted mechanical exfoliation from bulk crystals [31,32,33,34]. This method exploits the strong Au-S interaction to exfoliate large area (cm^2) MoS_2 membranes, predominantly formed by monolayers, on a gold substrate. These high crystalline quality membranes can be subsequently transferred on insulating substrates [33,34].

Using identical ALD conditions on 1L MoS_2 membranes supported by gold (MoS_2/Au) or by Al_2O_3 (100 nm)/Si substrate ($\text{MoS}_2/\text{Al}_2\text{O}_3/\text{Si}$), the typical inhomogeneous coverage by Al_2O_3 islands was observed in the case of the 1L $\text{MoS}_2/\text{Al}_2\text{O}_3/\text{Si}$ system, whereas the formation of a highly uniform Al_2O_3 insulating film (~ 3.6 nm thick) was observed on the 1L MoS_2/Au sample. This excellent uniformity is the result of an enhanced ALD nucleation on MoS_2 surface due to the interaction with Au substrate, giving rise to $\sim 50\%$ Al_2O_3 surface coverage after only 10 ALD cycles, and $>90\%$ coverage after 40 cycles. In this respect, micro-Raman and micro-photoluminescence spectroscopy analyses of 1L MoS_2/Au and 1L $\text{MoS}_2/\text{Al}_2\text{O}_3/\text{Si}$ samples before and after ALD processes provided an insight on the role of the substrate-related doping and strain in the Al_2O_3 nucleation and growth.

Experimental

The gold substrate used for MoS_2 mechanical exfoliation was prepared by sequentially depositing a 10 nm Ni adhesion layer and a 15 nm Au film with DC magnetron sputtering on top of a SiO_2/Si sample. This process resulted in a very smooth Au surface with RMS roughness (<0.2 nm), suitable for the MoS_2 exfoliation procedure [34]. This latter was performed by pressing a bulk molybdenite stamp on the surface of a freshly prepared Au/Ni/ SiO_2 sample, in order to avoid the adsorption of contaminants (e.g. adventitious carbon) on Au surface, which would reduce the 1L MoS_2 exfoliation yield [35]. This exfoliation results in a large area mostly composed 1L MoS_2 with some 2L regions identified by optical contrast, AFM and Raman spectroscopy.

The Al₂O₃/Si substrate used for transferring the Au-exfoliated MoS₂ was prepared by DC-pulsed RF reactive sputtering of 100 nm Al₂O₃ on a Si wafer. The transfer procedure of the large areas MoS₂ membranes from gold to this insulating substrate is discussed in details in Ref. [34].

Thermal ALD of Al₂O₃ thin films on MoS₂ was carried out in a PE-ALD LL SENTECH Instruments GmbH reactor, using TMA and H₂O as the aluminum precursor and co-reactant, respectively. All depositions were carried out at a temperature of 250 °C and with a pressure of 10 Pa. Initially, a process consisting of 80 ALD cycles was simultaneously carried out on both 1L MoS₂/Au and 1L MoS₂/Al₂O₃/Si systems, to compare the Al₂O₃ coverage uniformity. After observing the beneficial effect of the Au substrate on the uniformity of the Al₂O₃ growth on 1L MoS₂, the nucleation and growth mechanisms on the 1L MoS₂/Au were investigated in a more detail, by performing shorter ALD processes (10 and 40 deposition cycles).

The surface roughness, coverage fraction and thickness of the deposited Al₂O₃ on MoS₂ were evaluated by tapping mode Atomic Force Microscopy (AFM), morphology and phase, using a DI3100 equipment by Bruker with Nanoscope V electronics. Sharp silicon tips with a curvature radius of 5 nm were used for these measurements. Furthermore, the electrical insulating properties of the very thin Al₂O₃ films deposited on 1L MoS₂/Au were evaluated by conductive AFM (C-AFM) analyses [36] using the TUNA module and Pt-coated silicon tips.

Micro-Raman spectroscopy and micro-photoluminescence (PL) measurements of MoS₂ on the different substrates and before/after the ALD growth of Al₂O₃ were carried out using an Horiba HR-Evolution micro-Raman system with a confocal microscope (100× objective) and a laser excitation wavelength of 532 nm.

Results and discussion

Figure 1 shows the comparison between the AFM surface morphologies of Al₂O₃ simultaneously deposited at 250 °C by 80 ALD cycles on the surface of the 1L MoS₂/Al₂O₃/Si sample (a) and of the

1L MoS₂/Au sample (b), respectively. A very inhomogeneous Al₂O₃ coverage, resulting in a root mean square roughness RMS=2.5 nm, is observed on the surface of 1L MoS₂ transferred on the Al₂O₃/Si substrate. Furthermore, the height distribution in Fig.1 (c) shows two components, related to bare and Al₂O₃ covered MoS₂ areas, due to ~70% coverage and an average Al₂O₃ islands height of ~4 nm. This scenario, schematically depicted in the inset of Fig.1(c), is consistent with the commonly reported island growth during direct thermal ALD on MoS₂ surface. Differently, for 1L MoS₂ supported by the Au substrate (Fig.1(b)), a pinhole-free Al₂O₃ layer with a very flat morphology is observed after 80 ALD cycles. The deposited film exhibits a very narrow height distribution (Fig.1(d)) and low surface roughness (RMS= 0.25 nm), only slightly higher than the one measured on bare 1L MoS₂ on Au (RMS= 0.2 nm) [32]. Such morphological results suggest that, under identical process conditions, an enhanced Al₂O₃ nucleation occurs on the surface of 1L MoS₂ in contact with gold, resulting in the formation of a continuous Al₂O₃ film, as schematically depicted in the inset of Fig.1(d).

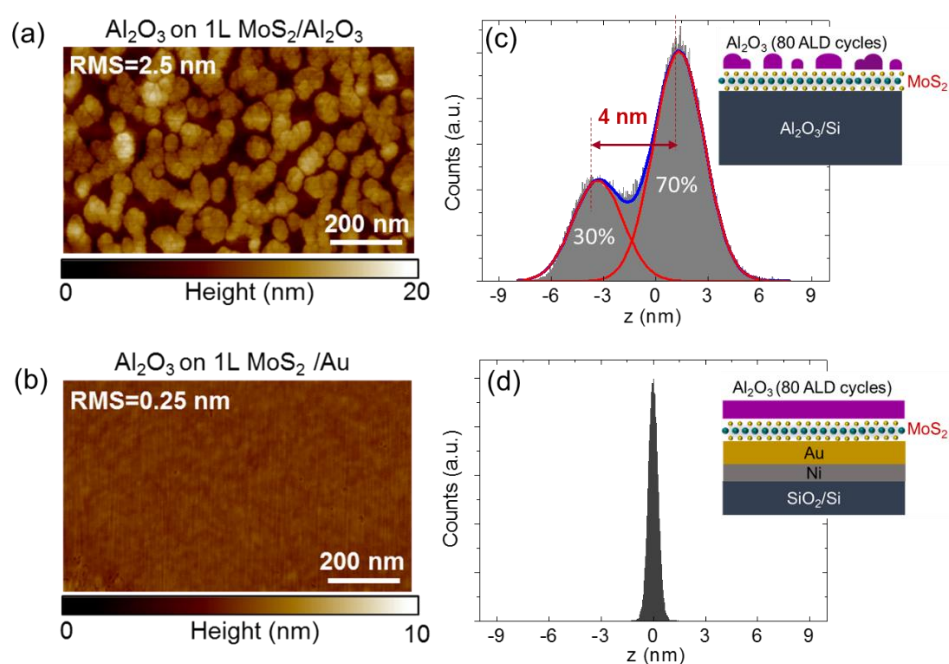


Fig. 1. AFM morphologies of Al₂O₃ simultaneously deposited at 250 °C by 80 ALD cycles on the surface of the 1L MoS₂/Al₂O₃/Si sample (a) and of the 1L MoS₂/Au sample (b). The root mean square (RMS) roughness values of the two samples are indicated. (c) Histogram of the height distribution obtained from the AFM map of Al₂O₃ on 1L MoS₂/Al₂O₃/Si, from which ~70% Al₂O₃ coverage and an average height ~4 nm of Al₂O₃ islands were evaluated. (d) Histogram of the height distribution for Al₂O₃ on 1L MoS₂/Au. The configuration of the deposited Al₂O₃ on 1L MoS₂/Al₂O₃/Si and 1L MoS₂/Au is schematically illustrated in the insets of panels (c) and (d).

In order to evaluate the thickness and the electrical insulating quality of the uniform Al₂O₃ film deposited on 1L MoS₂/Au, C-AFM morphology and current maps were simultaneously acquired by scanning the metal tip across a step between the Al₂O₃/1L MoS₂ stack and the underlying Au substrate, as schematically depicted in Fig.2(a). Fig.2(b) shows a morphological image collected in the proximity of a crack in the 1L MoS₂ membrane. The growth of a uniform and compact Al₂O₃ film on 1L MoS₂ and a poor ALD growth on the bare Au surface can be deduced from this image. Furthermore, the height line-profile in Fig.2 (c) displays a total thickness of the Al₂O₃/MoS₂ stack of ~4.3 nm, from which a deposited Al₂O₃ thickness of ~3.6 nm can be estimated, by subtracting the thickness of 1L MoS₂ on Au (~0.7 nm) [34]. The slightly increased height observed at the step edge can be ascribed to the folding of the broken 1L MoS₂ membrane. The very good electrical insulating properties of the 3.6 nm Al₂O₃ film deposited onto 1L MoS₂ on Au are demonstrated by the current map in Fig.2(d), acquired by applying a bias of 3 V between the tip and the gold substrate. In particular, the line-profile in Fig.2(e) shows very low current values (between 10 and 30 fA) in the Al₂O₃/1L MoS₂ region, whereas the saturation value of the current sensor was reached on Au region. The current conduction in the region close to the step edge suggests lower insulating properties of Al₂O₃ deposited on the locally folded MoS₂ membrane.

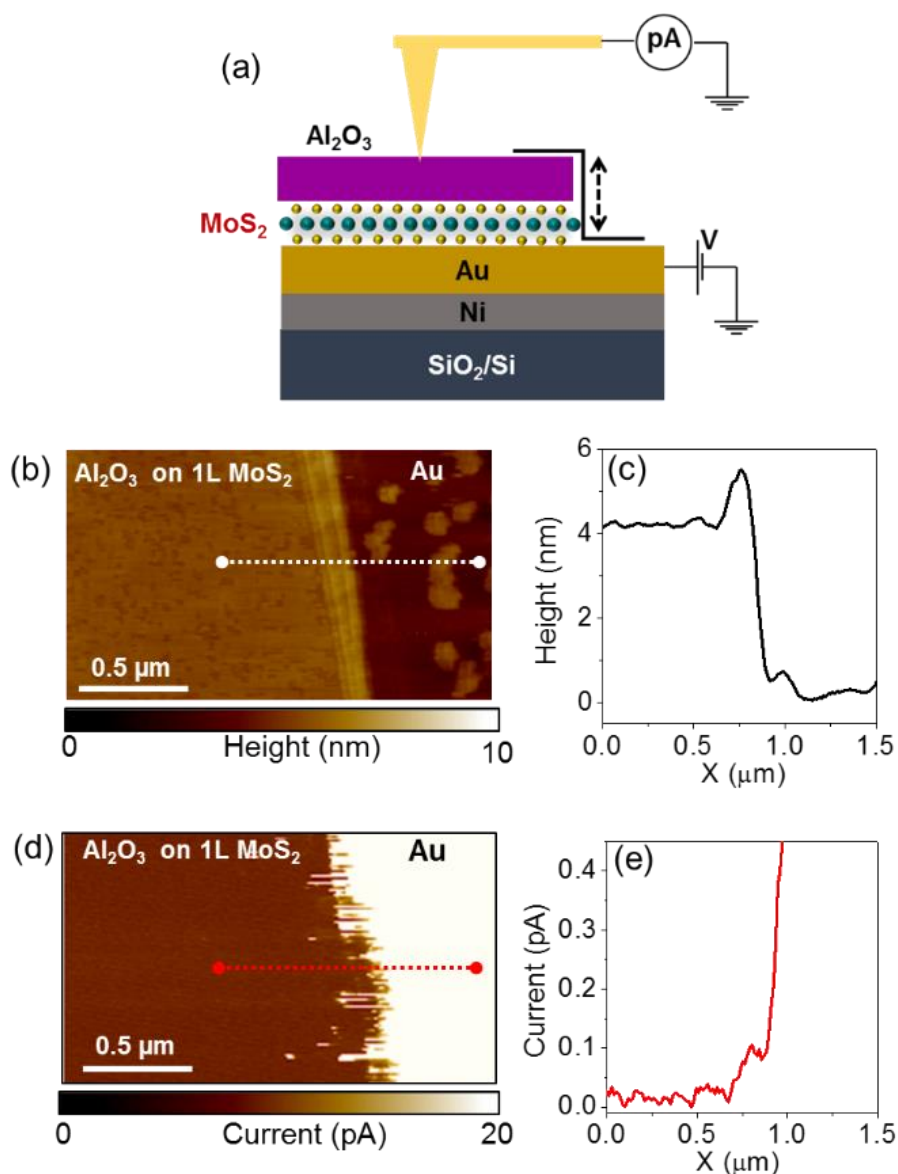


Fig.2 (a) Schematic of the step between the Al₂O₃/1L MoS₂ stack and the underlying Au substrate. (b) AFM image and (c) height line-profile of the step, from which a deposited Al₂O₃ thickness of ~3.6 nm was estimated, after subtracting 1L MoS₂ thickness (~0.7 nm) (d) C-AFM current map simultaneously acquired with a bias V=3V and (e) current profile, demonstrating a good insulating quality of the deposited Al₂O₃ film onto 1L MoS₂ on Au.

After demonstrating the formation of a homogeneous ~3.6 nm Al₂O₃ insulating film on top of 1L MoS₂/Au by 80 ALD cycles at 250 °C, we investigated the film nucleation and growth stages by AFM analyses performed after a reduced number of ALD cycles at the same temperature.

Fig.3(a) and (d) show two tapping mode morphological images acquired on 1L MoS₂/Au samples after 10 and 40 ALD cycles, respectively. In particular, after 10 cycles, a very irregular and ultrathin coating can be deduced from the morphological image, resulting in a RMS \approx 0.4 nm, slightly higher than the \sim 0.2 nm value measured on the bare 1L MoS₂/Au sample. On the other hand, a grain-shaped morphology of the deposited Al₂O₃ film can be clearly observed after 40 ALD cycles (see Fig.3(d)), suggesting the occurrence of 3D growth of Al₂O₃ islands on top of the inhomogeneous nucleation layer formed at lower number of cycles. A quantification of the coverage percentage is very difficult from these morphological images. On the other hand, the Al₂O₃ coated and uncoated 1L MoS₂ areas can be clearly distinguished in the corresponding AFM phase maps (Fig.3(b) and (e)), as the phase signal is known to be very sensitive to the surface properties of materials. In particular, the red and black contrast in these two images correspond to the Al₂O₃-covered and uncovered 1L MoS₂, respectively. Furthermore, the histograms of the phase distribution extracted from the two maps are reported in Fig.3(c) and (f), from which an Al₂O₃ coverage percentage of 50% and 93% were evaluated after 10 and 40 ALD cycles, respectively. This very high coverage after only 40 ALD cycles, corresponding to \sim 1.4 nm Al₂O₃ thickness (measured by an AFM step-height analysis as in Fig.2(b)), demonstrates a very good nucleation on Au supported 1L MoS₂.

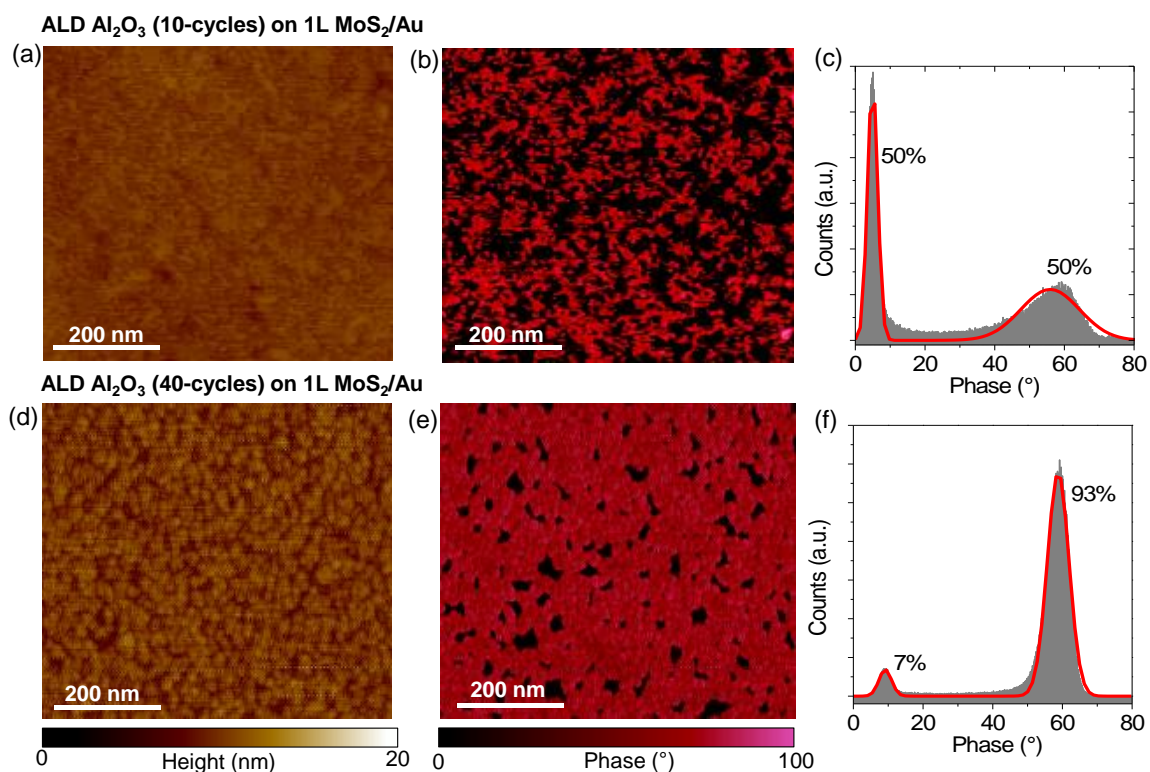


Figure 3 (a) AFM morphology and (b) phase map measured after 10 Al_2O_3 ALD cycles on 1L MoS_2/Au . (c) Histogram of the phase distribution and evaluation of the Al_2O_3 coverage percentage on the same sample. (d) AFM morphology and (e) phase map measured after 40 Al_2O_3 ALD cycles on 1L MoS_2/Au . (f) Histogram of the phase distribution and evaluation of the Al_2O_3 coverage percentage on the same sample

Interestingly, the coverage degree was found to be strongly dependent on the number of MoS_2 layers on which the ALD process is performed. Fig.4 shows a representative AFM morphology (a) and phase image (b) collected after 40 ALD cycles in a region of the exfoliated MoS_2 membrane on Au including 1L and 2L MoS_2 areas. A very different Al_2O_3 coverage can be clearly observed (especially in the phase image) on 1L and 2L MoS_2 regions, with a much denser Al_2O_3 nucleation on 1L than on the 2L MoS_2 .

This observation further confirms the key role played by the interaction at MoS_2/Au interface on the ALD nucleation on top of MoS_2 . As schematically illustrated in Fig.4(c), left image, the strongly polarized Au-S bond is expected to significantly affect the electronic and vibrational properties of the first MoS_2 layer closely in contact with the substrate, which can be responsible of the observed

enhanced ALD nucleation on 1L-MoS₂. On the other hand, in the case of 2L MoS₂ (Fig.4(c), right image), the Au-S interaction is expected to be partially screened by the presence of the first MoS₂ layer, resulting in a less-efficient ALD growth. A similar degradation of Al₂O₃ coverage homogeneity has been also observed in the case of bilayer or few-layers CVD graphene on the native copper substrate [26] and of bilayer epitaxial graphene on 4H-SiC(0001) [27].

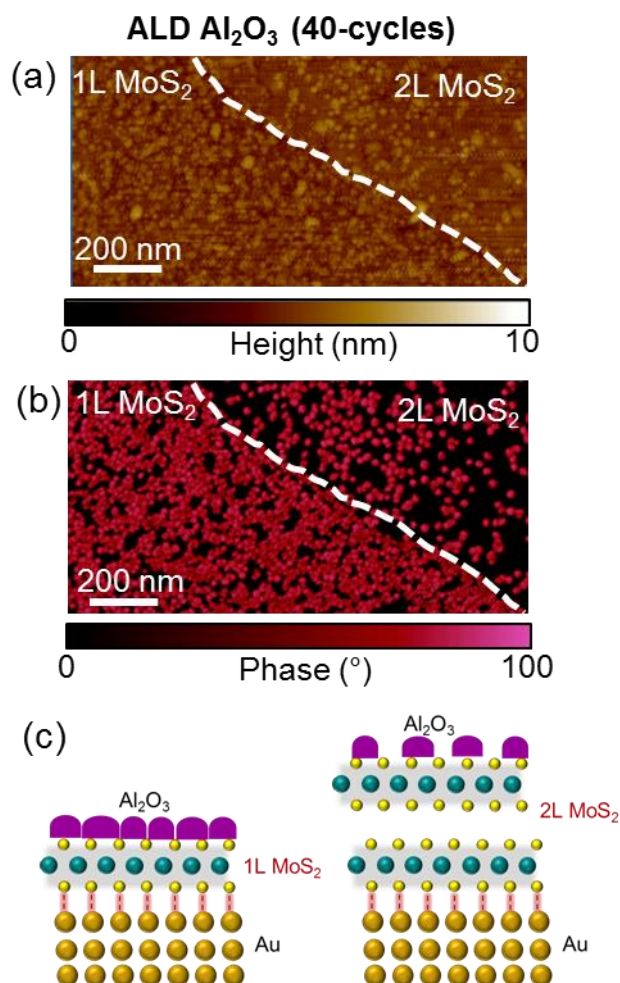


Fig.4: AFM-morphology (a) and phase image (b) of Al₂O₃ deposited by 40 ALD cycles on a region including both 1L and 2L MoS₂ on Au. (c) Schematic illustration of the impact of Au-S interaction on the ALD nucleation on 1L- and 2L MoS₂.

Then, micro-Raman spectroscopy analyses have been performed to investigate the strain and doping status of 1L MoS₂ residing on Au and Al₂O₃ substrates before and after the ALD growth. Fig.5(a) reports two representative Raman spectra for as-exfoliated 1L MoS₂ on Au (reference) and after 80

TMA/H₂O ALD cycles, resulting in the homogeneous ~3.6 nm Al₂O₃ film deposition shown in Fig. 2(b). The corresponding Raman spectra for 1L MoS₂ transferred onto the Al₂O₃/Si substrate (reference) and after the 80 ALD cycles are shown in Fig.5(b). From the comparison of the reference spectra on the two substrates, a significantly higher separation $\Delta\omega$ between the in-plane (E') and out-of-plane (A₁') vibrational peaks is observed for 1L MoS₂ on Au ($\Delta\omega\approx 21\text{ cm}^{-1}$) as compared to the case of 1L MoS₂ on Al₂O₃/Si ($\Delta\omega\approx 18\text{ cm}^{-1}$). Such a difference is due to significant red-shift of the E' peak (mostly associated to the strain) and to a slight blue shift of the A₁' peak (mostly related to the doping) for 1L MoS₂ membrane on gold. Interestingly, the E' peak red-shift is further increased and the A₁' peak blue-shift is slightly reduced after ALD of the uniform Al₂O₃ film on the gold supported membrane. On the other hand, only a slight red shift of the A₁' peak was observed after 80 ALD cycles on the Al₂O₃ supported 1L MoS₂, probably due to the inhomogeneous Al₂O₃ coverage (as shown in Fig.1(a)). In order to achieve a quantification of the strain ε (%) and doping n (cm⁻²) for the 1L MoS₂ membranes on the two different substrates before and after the ALD process, a correlative analysis of the A₁' vs E' peak frequencies has been carried out in Fig.5(c), according to the procedure recently discussed in Ref. [34]. The red and black lines in Fig.5(c) represent the theoretical behaviour of the peaks' frequencies for 1L MoS₂ subjected only to a biaxial strain (tensile or compressive) or to doping (n-type or p-type), respectively. The crossing point (gray square) of these lines corresponds to literature values of the E' and A₁' positions for a free-standing 1L MoS₂, taken as the best approximation for ideally unstrained and undoped MoS₂. The spacing of the dashed lines parallel to the ideal strain and doping lines is associated with carrier density changes of $0.1\times 10^{13}\text{ cm}^{-2}$ and strain changes of 0.1%, respectively. The black point is the average value of the A₁' vs E' frequencies from several (>20) Raman spectra measured on the reference 1L MoS₂/Au sample, whereas the error bars are the standard deviations from this statistical analysis. The magenta point is the average value obtained from Raman analyses on several points of the reference 1L MoS₂/Al₂O₃ sample. For this sample, the A₁' frequency exhibits a significant dispersion (indicated by the error bar), whereas the small E' frequency dispersion is within the data point. According to the graphical analysis in Fig.5(c),

the reference 1L MoS₂/Au sample is characterized by an average tensile strain of $\varepsilon \approx 0.21\%$ and p-type doping of $n \approx -0.25 \times 10^{13} \text{ cm}^{-2}$, whereas an opposite compressive strain $\varepsilon \approx -0.25\%$ and n-type doping $n \approx 0.5 \times 10^{13} \text{ cm}^{-2}$ are observed for 1L MoS₂ transferred onto the Al₂O₃/Si substrate. Such n-type behaviour is consistent with the unintentional doping type commonly reported for exfoliated or CVD-grown MoS₂, which has been associated to the presence of defects (e.g. sulphur vacancies) or to other impurities in the MoS₂ lattice [37,38]. In the case of 1L MoS₂ on Au, a strong electron transfer to the substrate is guessed, which overcompensates the native n-type doping, resulting in a net p-type behaviour. Furthermore, the tensile strain for 1L MoS₂ on Au can be ascribed to the lattice mismatch between MoS₂ and the Au surface, mostly exposing (111) orientation [39,40]. The opposite strain and doping status of 1L MoS₂/Al₂O₃ and 1L MoS₂/Au can be the explanation of the very different Al₂O₃ coverage observed in the two systems under identical thermal ALD conditions.

Noteworthy, the blue point in Fig.5(c) obtained from Raman analyses after 80 ALD cycles on 1L MoS₂/Au indicates a further increase of the tensile strain ($\varepsilon \approx 0.65\%$), as compared to the original value of 0.21%, which can be associated to the formation of a compact Al₂O₃ film on top of MoS₂. On the other hand, no significant changes with respect to the original p-type doping value was observed after the ALD growth, confirming that the doping status of the film is strongly dominated by the strong Au-1L MoS₂ interaction. Finally, the data-point for the 1L MoS₂/Al₂O₃ sample after the 80 ALD cycles indicates no significant changes in the tensile strain, consistently with the highly inhomogeneous Al₂O₃ coverage, and an increase of the n-type doping to $n \approx 0.6 \times 10^{13} \text{ cm}^{-2}$. This latter can be ascribed to positively charged defects [41] at the interface between the poor quality Al₂O₃ film and 1L MoS₂.

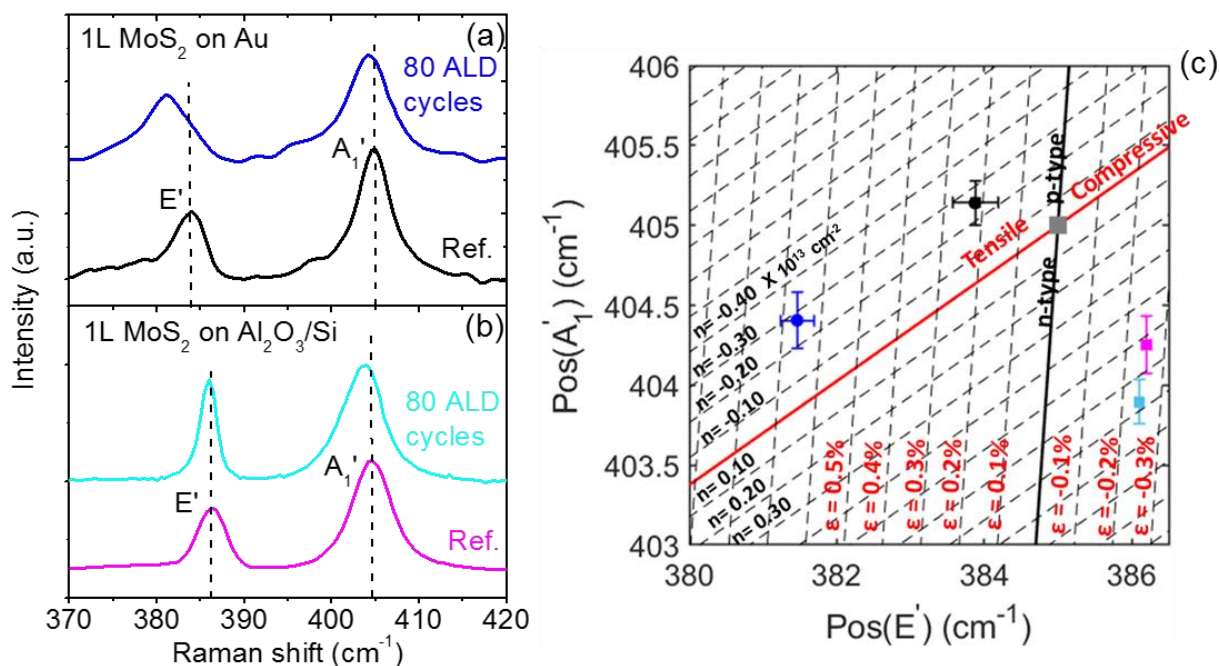


Figure 5 Representative Raman spectra collected on 1L MoS₂ on Au (a) and 1L MoS₂ on Al₂O₃/Si (b) before (reference) and after 80 Al₂O₃ ALD cycles. (c) Correlative plot of the A₁' vs E' peak frequencies of the Raman spectra acquired on the 1L MoS₂ on Au before (black circle) and after (blue circle) ALD deposition and for 1L MoS₂ on Al₂O₃/Si before (magenta square) and after (cyan square) ALD deposition, allowing to evaluate the type and average values of strain and doping of 1L MoS₂ membrane.

Raman analyses clearly show very different strain and doping properties of 1L MoS₂ residing on the Au and Al₂O₃/Si substrates, which finally result in the growth of different quality Al₂O₃ films after ALD deposition.

In Fig.6, micro-PL spectra acquired on the two reference 1L MoS₂ samples and after 80 cycles ALD growth are also reported, to further elucidate the impact of the substrate and of the deposition process on the optical emission properties of the direct bandgap 1L MoS₂ membrane.

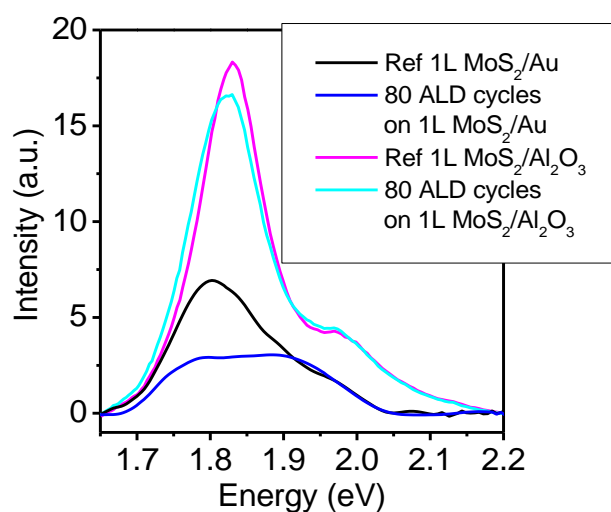


Figure 6 Micro-PL spectra acquired on 1L MoS₂/Al₂O₃ and on 1L MoS₂/Au samples before (ref. spectra) and after 80 Al₂O₃ ALD cycles.

A prominent emission peak located at 1.84 eV can be observed for 1L MoS₂ supported by Al₂O₃/Si, whereas a significant reduction of the PL intensity accompanied by the red shift of the main peak position at 1.79 eV is found for the reference sample on Au. A similar quenching of the PL intensity has been reported for 1L MoS₂ exfoliated on Au [34,35] and for MoS₂ functionalized with Au nanoparticles [42]. This behavior can be explained in terms of a preferential transfer of photoexcited charges from MoS₂ to Au. In addition, the tensile strain of 1L MoS₂ in contact with Au can also play a role in the reduction of the PL yield [43]. After 80 ALD cycles, only a small reduction of the PL intensity was observed for the 1L MoS₂/Al₂O₃ sample, which can be explained by the highly inhomogeneous Al₂O₃ coverage and to the small interaction of MoS₂ with the dielectric substrate. On

the other hand, further quenching of the PL intensity was found in the case of 1L MoS₂/Au sample covered by the ~3.6 nm uniform Al₂O₃ film. This observation can be consistent with the increase of the tensile strain observed by Raman analyses and to the increase of the interaction with the Au substrate due to the material added on top of MoS₂.

Conclusion

In conclusion, we have demonstrated the direct thermal ALD growth at 250 °C of highly homogeneous and ultra-thin (~3.6 nm) Al₂O₃ films with excellent insulating properties onto a monolayer MoS₂ membrane exfoliated on gold. Differently from the case of 1L MoS₂ supported by a common insulating substrate (Al₂O₃/Si), an enhanced nucleation of the high-*k* films was observed on the 1L MoS₂/Au system since the early stages of the ALD process, with the Al₂O₃ surface coverage increasing from ~50% (after only 10 ALD cycles) to >90% (after 40 cycles), up to the final ~3.6 nm uniform film (after 80 cycles). The coverage percentage was found to be significantly reduced in the case of 2L MoS₂/Au, indicating a crucial role of the S-Au interaction at the interface in the observed phenomena. Raman spectroscopy and PL analyses provided an insight about the role played by the tensile strain and p-type doping of 1L MoS₂ induced by the gold substrate on the enhanced high-*k* nucleation on MoS₂ surface.

The demonstrated high quality ALD growth of high-*k* dielectrics on large area 1L MoS₂ produced by the Au-assisted exfoliation can find important device applications, including the fabrication of FETs by optimized transfer of the Al₂O₃/1L MoS₂ stack onto an insulating substrate, or the passivation of non-volatile switching memory devices based on Au/1L MoS₂/Au junctions.

Acknowledgements

The authors acknowledge S. Di Franco (CNR-IMM) for the expert assistance in the sample preparation, P. Fiorenza and G. Greco (CNR-IMM) for useful discussions. This paper has been supported, in part, by MUR in the framework of the FlagERA- 732JTC 2019 project “ETMOS”. E.S.

acknowledges the PON project EleGaNTe (ARS01_01007) for financial support. Part of the experiments have been carried out using the facilities of the Italian Infrastructure Beyond Nano.

Received: ((will be filled in by the editorial staff))

Revised: ((will be filled in by the editorial staff))

Published online: ((will be filled in by the editorial staff))

References

- ¹ K. F. Mak, C. Lee, J. Hone, J. Shan, T. F. Heinz, Atomically Thin MoS₂: A New Direct-Gap Semiconductor, *Phys. Rev. Lett.* **2010**, *105*, 136805.
- ² A. Splendiani, L. Sun, Y. Zhang, T. Li, J. Kim, C.-Y. Chim, G. Galli, F. Wang, Emerging Photoluminescence in Monolayer MoS₂, *Nano Lett.* **2010**, *10*, 1271-1275.
- ³ Y. Y. Illarionov, T. Knobloch, M. Jech, M. Lanza, D. Akinwande, M. I. Vexler, T. Mueller, M. C. Lemme, G. Fiori, F. Schwierz, T. Grasser, Insulators for 2D nanoelectronics: the gap to bridge, *Nat. Commun.* **2020**, *11*, 3385.
- ⁴ F. Giannazzo, Engineering 2D heterojunctions with dielectrics, *Nat. Electron.* **2019**, *2*, 54–55.
- ⁵ F. Giannazzo, G. Greco, F. Roccaforte, S.S. Sonde, Vertical Transistors Based on 2D Materials: Status and Prospects, *Crystals* **2018**, *8*, 70.
- ⁶ B. Radisavljevic, A. Radenovic, J. Brivio, V. Giacometti, A Kis, Single-layer MoS₂ transistors, *Nature Nanotech.* **2011**, *6*, 147-150.
- ⁷ H. Liu, P. D. Ye, MoS₂ Dual-Gate MOSFET with Atomic-Layer-Deposited Al₂O₃ as Top-Gate Dielectric, *IEEE Electron Device Lett.* **2011**, *33*, 546–548.
- ⁸ A. Pakalla, M. Putkonen, in *Handbook of Deposition Technologies for Films and Coatings, 3rd Ed.*, Elsevier, **2010**, pp. 364–391.
- ⁹ H. Liu, K. Xu, X. Zhang, P. D. Ye, The integration of high-k dielectric on two-dimensional crystals by atomic layer deposition, *Appl. Phys. Lett.* **2012**, *100*, 152115.
- ¹⁰ T. Park, H. Kim, M. Leem, W. Ahn, S. Choi, J. Kim, J. Uh, K. Kwon, S.-J. Jeong, S. Park, Y. Kim, H. Kim, Atomic layer deposition of Al₂O₃ on MoS₂, WS₂, WSe₂, and h-BN: surface coverage and adsorption energy, *RSC Adv.* **2017**, *7*, 884–889.

-
- ¹¹ S. McDonnell, B. Brennan, A. Azcatl, N. Lu, H. Dong, C. Buie, J. Kim, C. L. Hinkle, M. J. Kim, R. M. Wallace, HfO₂ on MoS₂ by Atomic Layer Deposition: Adsorption Mechanisms and Thickness Scalability, *ACS Nano* **2013**, *7*, 10354–10361.
- ¹² T. Nam, S. Seo, H. Kim, Atomic layer deposition of a uniform thin film on two-dimensional transition metal dichalcogenides, *J. Vac. Sci. Technol. A* **2020**, *38*, 030803.
- ¹³ R. H. J. Vervuurt, W. M. M. Kessels, A. A. Bol, *Adv. Mater. Interfaces* **2017**, *4*, 1700232.
- ¹⁴ E. Schilirò, R. Lo Nigro, F. Roccaforte, F. Giannazzo, Recent advances in seeded and seed-layer-free atomic layer deposition of high-K dielectrics on graphene for electronics, *C - J. Carbon Res.* **2019**, *5*, 53.
- ¹⁵ F. Giannazzo, E. Schilirò, R. Lo Nigro, F. Roccaforte, R. Yakimova, Atomic layer deposition of high-k insulators on epitaxial graphene: a review, *Appl. Sci.* **2020**, *10*, 2440.
- ¹⁶ G. Fisichella, E. Schilirò, S. Di Franco, P. Fiorenza, R. Lo Nigro, F. Roccaforte, S. Ravesi, F. Giannazzo, Interface electrical properties of Al₂O₃ thin films on graphene obtained by atomic layer deposition with an in situ seedlike layer, *ACS Appl. Mater. Interfaces* **2017**, *9*, 7761–7771.
- ¹⁷ Y.-S. Lin, P.-H. Cheng, K.-W. Huang, H.-C. Lin, M.-J. Chen, Atomic layer deposition of sub-10 nm high-*k* gate dielectrics on top-gated MoS₂ transistors without surface functionalization, *Applied Surface Science* **2018**, *443*, 421–428.
- ¹⁸ A. Iraiwa, D. Matsumura, H. Kawarada, *J. Appl. Phys.* **120**, 084504 (2016)
- ¹⁹ L. Cheng, X. Qin, A. T. Lucero, A. Azcatl, J. Huang, R. M. Wallace, K. Cho, J. Kim., Atomic Layer Deposition of a High-k Dielectric on MoS₂ Using Trimethylaluminum and Ozone, *ACS Appl. Mater. Interfaces* **2014**, *6*, 11834–11838
- ²⁰ J. Yang, S. Kim, W. Choi, S. H. Park, Y. Jung, M.-H. Cho, H. Kim., Improved Growth Behavior of Atomic-Layer-Deposited High-k Dielectrics on Multilayer MoS₂ by Oxygen Plasma Pretreatment, *ACS Appl. Mater. Interfaces* **2013**, *5*, 4739–4744.
- ²¹ B. Huang, M. Zheng, Y. Zhao, J. Wu, J. T. L. Thong, Atomic Layer Deposition of High-Quality Al₂O₃ Thin Films on MoS₂ with Water Plasma Treatment, *ACS Appl. Mater. Interfaces* **2019**, *11*, 35438–35443.
- ²² K. M. Price, K. E. Schauble, F. A. McGuire, D. B. Farmer, A. D. Franklin, Uniform Growth of Sub-5-Nanometer High- κ Dielectrics on MoS₂ Using Plasma-Enhanced Atomic Layer Deposition, *ACS Appl. Mater. Interfaces* **2017**, *9*, 23072–23080.
- ²³ K. M. Price, S. Najmaei, C. E. Ekuma, R. A. Burke, M. Dubey, A. D. Franklin, Plasma-Enhanced Atomic Layer Deposition of HfO₂ on Monolayer, Bilayer, and Trilayer MoS₂ for the Integration of High- κ Dielectrics in Two-Dimensional Devices, *ACS Appl. Nano Mater.* **2019**, *2*, 4085–4094.

- ²⁴ C. Wirtz, T. Hallam, C. P. Cullen, N. C. Berner, M. O'Brien, M. Marcia, A. Hirsch, G S. Duesberg, Atomic layer deposition on 2D transition metal chalcogenides: layer dependent reactivity and seeding with organic ad-layers, *Chem. Commun.* **2015**, *51*, 16553
- ²⁵ H. Zhang, G. Arutchelvan, J. Meersschaut, A. Gaur, T. Conard, H. Bender, D. Lin, I. Asselberghs, M. Heyns, I. Radu, W. Vandervorst, A. Delabie, MoS₂ Functionalization with a Sub-nm Thin SiO₂ Layer for Atomic Layer Deposition of High-κ Dielectrics, *Chem. Mater.* **2017**, *29*, 6772–6780.
- ²⁶ B. Dlubak, P.R. Kidambi, R.S. Weatherup, S. Hofmann, J. Robertson, *Appl. Phys. Lett.*, *100*, p. 173113 (2012).
- ²⁷ E. Schilirò, R. Lo Nigro, F. Roccaforte, I. Deretzis, A. La Magna, A. Armano, S. Agnello, B. Pecz, I.G. Ivanov, R. Yakimova, F. Giannazzo, *Adv. Mater. Interfaces* 1900097 (2019).
- ²⁸ A. J. Pollard, E. W. Perkins, N. A. Smith, A. Saywell, G. Goretzki, A. G. Phillips, S. P. Argent, H. Sachdev, F. Muller, S. Hufner, S. Gsell, M. Fischer, M. Schreck, J. Osterwalder, T. Greber, S. Berner, N. R. Champness, and P. H. Beton, Supramolecular Assemblies Formed on an Epitaxial Graphene Superstructure, *Angew. Chem. Int. Ed.* **2010**, *49*, 1794
- ²⁹ H. Zhang, J. Sun, T. Low, L. Zhang, Y. Pan, Q. Liu, J. Mao, H. Zhou, H. Guo, S. Du, F. Guinea, and H.-J. Gao, Assembly of iron phthalocyanine and pentacene molecules on a graphene monolayer grown on Ru(0001), *Phys. Rev. B* **2011**, *84*, 245436.
- ³⁰ E. Schilirò, R. Lo Nigro, S.E. Panasci, F.M. Gelardi, S. Agnello, R. Yakimova, F. Roccaforte, F. Giannazzo, Aluminum oxide nucleation in the early stages of atomic layer deposition on epitaxial graphene, *Carbon* **2020**, *169*, 172-181.
- ³¹ S. R. Desai, S. R. Madhvapathy, M. Amani, D. Kiriya, M. Hettick, M. Tosun, Y. Zhou, M. Dubey, J. W. Ager, D. Chrzan, A. Javey, Gold-Mediated Exfoliation of Ultralarge Optoelectronically-Perfect Monolayers, *Advanced Materials* **2016**, *28*, 4053-4058.
- ³² Y. Huang, Y.-H. Pan, R. Yang, L.-H. Bao, L. Meng, H.-L. Luo, Y.-Q. Cai, G.-D. Liu, W.-J. Zhao, Z. Zhou, L.-M. Wu, Z.-L. Zhu, M. Huang, L.-W. Liu, L. Liu, P. Cheng, K.-H. Wu, S.-B. Tian, C.-Z. Gu, Y.-G. Shi, Y.-F. Guo, Z. G. Cheng, J.-P. Hu, L. Zhao, G.-H. Yang, E. Sutter, P. Sutter, Y.-L. Wang, W. Ji, X.-J. Zho, H.-J. Gao, Universal mechanical exfoliation of large-area 2D crystals, *Nature Commun.* **2020**, *11*, 2453.
- ³³ F. Liu, W. Wu, Y. Bai, S. H. Chae, Q. Li, J. Wang, J. Hone, X.-Y. Zhu, Disassembling 2D Van der Waals Crystals into Macroscopic Monolayers and Reassembling into Artificial Lattices, *Science* **2020**, *367*, 903–906.
- ³⁴ S.E. Panasci, E. Schilirò, G. Greco, M. Cannas, F. M. Gelardi, S. Agnello, F. Roccaforte, F. Giannazzo, Strain, doping and electronic transport of large area monolayer MoS₂ exfoliated on gold and transferred to an insulating substrate, *ACS Appl. Mater. Interfaces* (2021). DOI: acsami.1c05185.

-
- ³⁵ M. Velický, G. E. Donnelly, W. R. Hendren, S. McFarland, D. Scullion, W. J. I. De Benedetti, G. C. Correa, Y. Han, A. J. Wain, M. A. Hines, D. A. Muller, K. S. Novoselov, H. D. Abruña, R. M. Bowman, E. J. G. Santos, F. Huang, Mechanism of Gold-Assisted Exfoliation of Centimeter- Sized Transition-Metal Dichalcogenide Monolayers, *ACS Nano* **2018**, *2*, 10463-10472.
- ³⁶ F. Giannazzo, E. Schilirò, G. Greco, F. Roccaforte, Conductive Atomic Force Microscopy of Semiconducting Transition Metal Dichalcogenides and Heterostructures, *Nanomaterials* **2020**, *10*, 803.
- ³⁷ F. Giannazzo, G. Fisichella, A. Piazza, S. Agnello, F. Roccaforte, Nanoscale Inhomogeneity of the Schottky Barrier and Resistivity in MoS₂ Multilayers, *Phys. Rev. B* **2015**, *92*, 081307(R)
- ³⁸ F. Giannazzo, G. Fisichella, G. Greco, S. Di Franco, I. Deretzis, A. La Magna, C. Bongiorno, G. Nicotra, C. Spinella, M. Scopelliti, B. Pignataro, S. Agnello, F. Roccaforte, Ambipolar MoS₂ Transistors by Nanoscale Tailoring of Schottky Barrier Using Oxygen Plasma Functionalization, *ACS Appl. Mater. Interfaces* **2017**, *9*, 23164–23174.
- ³⁹ C. Gong, C. Huang, J. Miller, L. Cheng, Y. Hao, D. Cobden, J. Kim, R. S. Ruoff, R. M. Wallace, K. Cho, X. Xu, Y. J. Chabal, Metal contacts on physical vapor deposited monolayer MoS₂, *ACS Nano* **2013**, *7*, 11350–11357.
- ⁴⁰ A. Bruix, J. A. Miwa, N. Hauptmann, D. Wegner, S. Ulstrup, S. S. Grønberg, C. E. Sanders, M. Dendzik, A. Grubisic Cabo, M. Bianchi, J. V. Lauritsen, A. A. Khajetoorians, B. Hammer, P. Hofmann, Single-layer MoS₂ on Au(111): Band gap renormalization and substrate interaction, *Phys. Rev. B* **2016**, *93*, 165422.
- ⁴¹ E. Schilirò, P. Fiorenza, C. Bongiorno, C. Spinella, S. Di Franco, G. Greco, R. Lo Nigro, F. Roccaforte, Correlating electron trapping and structural defects in Al₂O₃ thin films deposited by plasma enhanced atomic layer deposition, *AIP Advances* **2020**, *10*, 125017.
- ⁴² U. Bhanu, M. R. Islam, L. Tetard, S. I. Khondaker, Photoluminescence Quenching in Gold-MoS₂ Hybrid Nanoflakes, *Scientific Reports* **2015**, *4*, 5575.
- ⁴³ D. Lloyd, X. Liu, J. W. Christopher, L. Cantley, A. Wadehra, B. L. Kim, B. B. Goldberg, A. K. Swan, J. S. Bunch, Band Gap Engineering with Ultralarge Biaxial Strains in Suspended Monolayer MoS₂. *Nano Lett.* **2016**, *16*, 5836–5841.